Microstructural and mechanical characterization of electron beam welded Al-alloy 7020

Article *in* Journal of Materials Science · June 2007

DOI: 10.1007/s10853-007-1604-z

2 authors:

Gürel Çam
Iskenderun Technical University
90 PUBLICATIONS **2,706** CITATIONS

SEE PROFILE

M. Koçak
Gedik Holding, Gedik University
186 PUBLICATIONS **2,965** CITATIONS

SEE PROFILE

J Mater Sci (2007) 42:7154–7161
DOI 10.1007/s10853-007-1604-z

Microstructural and mechanical characterization of electron beam welded Al-alloy 7020

G. Çam · M. Koçak

Received: 6 March 2006 / Accepted: 12 February 2007 / Published online: 10 May 2007

Abstract The electron beam (EB) welding process is used to weld any metal that can be arc welded with equal or superior weld quality. EB welding is carried out in a high-purity vacuum environment, which results in freedom from impurities such as oxides and nitrides. Thus, pore-free joints can readily be achieved in metallic materials, such as Al-alloys and Ti-alloys. However, autogenous EB welding of some aluminium alloys leads to a significant strength reduction (undermatching) in the fusion zone due to the loss of strengthening phases. For such Al-alloys, the local microstructure-property relationships should be established to satisfy the service requirement of a welded component with strength undermatching. Autogenous EB welding was performed on 5 mm thick aluminium alloy 7020 plate. Microstructural characterization of the weld metals was made by optical and scanning electron microscopy. Extensive microhardness measurements were conducted in the weld regions of the joints which exhibited a hardness loss in the fusion zone due to the loss of strengthening phases. Tensile properties of the joints were determined by testing flat transverse tensile specimens at room temperature without machining the weld profiles. Furthermore, elastic-plastic fracture toughness tests (CTOD) were carried out on the base material and welded joints at room temperature.

G. Çam (✉)
Faculty of Engineering and Architecture,
Mechanical Engineering Department, Mustafa Kemal University, 31034 Antakya, Turkey
e-mail: gcam@mku.edu.tr

M. Koçak
GKSS Research Center, Institute of Materials Research,
Max-Planck-Str., 21502 Geesthacht, Germany

Introduction

The electron beam (EB) welding process offers several unique advantages, such as low distortion, low residual stresses, deep penetration, and narrow bead and HAZ widths compared to other conventional welding processes. Its ability to achieve a high weld depth-to width ratio eliminates the need for multiple-pass welds in contrast to arc welding. Moreover, its ability to employ high welding speeds, as a result of the high melting rates associated with the concentrated heat source, reduces the time required to accomplish the welding (the formation of narrow fusion and HAZ regions), thereby leading to an increased productivity and higher efficiency. Consequently, this high power density welding process is increasingly applied for manufacturing a wide range of engineering components using Ti-alloys, Al-alloys, and steels. Of particular interest is the ability to join the more difficult aerospace alloys with minimal component distortion and high reproducibility of joint quality.

Joining of Al-alloys present some difficulties, such as the removal of stable oxide layer from the surfaces in diffusion bonding and porosity formation as well as occurrence of hot cracking in fusion welding, i.e. arc welding and laser beam welding [1–5]. Proper cleaning and shielding are normally utilized in welding of aluminium alloys to ensure the production of welds free of gas porosity. Diamond machining just before welding was found to minimize pores in the weld metal of aluminium alloy 5083 joined by electron beam welding [6]. A certain

amount of porosity (provided that the pores are small in size and uniformly distributed) can perhaps be allowed in non-critical weld joints without significant deterioration of joint performance. The EB welding process is carried out in a high-purity vacuum environment, which results in freedom from impurities such as oxides and nitrides. Thus, pore-free joints can be achieved in metallic materials, such as Ti-alloys and Al-alloys. Significant progress has been made in understanding the weldability and characterization aspects of various metallic materials welded by this process.

There is no publication in the literature on EB welding of alloy 7020. The chemical composition of the alloy used in the present study consists of 1.25 wt% Mg, 4.32 wt% Zn, 0.14 wt% Zr, 0.12 wt% Si, 0.29 wt% Fe, 0.12 wt% Cu, 0.29 wt% Mn, 0.13 wt% Cr, 0.004 wt% Ni and 0.028 wt% Ti. This particular alloy containing a low amount of Cu (i.e. 0.12 wt %) has a narrow melting range and is thus not very sensitive to cracking in welding. Moreover, the high thermal gradient from the weld into the base metal in EB welding (minimal heat input) creates very limited metallurgical modifications and crack sensitivity is, therefore, reduced. Furthermore, the 7xxx series alloys possess the ability to naturally age in the HAZ. The recovery of strength by natural aging is similar to post-weld artificial aging, but the time required is substantial, i.e. 14 days. However, due to the very high temperatures experienced in the fusion zone, the loss of some elements, e.g. Mg, occur during EB welding. This also leads to the fact that the strength of the fusion zone cannot be restored to that of the base metal by post-weld heat treatment. Cieslak and Fuerschbach [7] have, for example, proposed Mg evaporation during laser beam welding of alloy 6061 leading to loss of strength in the fusion zone.

In the present study, the results of microstructural characterization and mechanical tests conducted on EB welded alloy 7020 plate, which is a heat treatable alloy and its strength is derived from fine Mg_2Zn precipitates and the solid solution of Mg, to establish the local microstructure-property relationship of this joint have been discussed. A very low level of porosity has been achieved owing to the surface cleaning prior to welding and the vacuum environment of the EB welding process. Moreover, the influence of strength loss in the fusion zone on the fracture properties was determined. The fracture toughness of the EB weld was found to be higher than that of the base plate due to the loss of strength in the fusion zone.

Experimental procedure

In this study, an Al–Zn–Mg (7xxx series) alloy, i.e. alloy 7020 plate (in T6 condition: solution heat treated and artificially aged) with a thickness of 5 mm was welded by electron beam welding with a travel speed of 1.5 m/min. The plate surfaces and weld edges were mechanically and chemically etched prior to welding. The accelerating voltage and beam current used were 50 kV and 120 mA, respectively. Extensive optical and scanning electron microscopy including EDX analyses were conducted to investigate the microstructural changes taking place in the HAZ and fusion zone (FZ). A scanning electron microscope of 30 kV with a facility of energy dispersive spectroscopy (EDS) was used in this study.

All mechanical tests were conducted well after 14 days following the welding, allowing for natural aging. Therefore, no further aging is to be expected in the fusion zone of the joint. Extensive microhardness measurements were conducted across the joint in three locations (i.e. top, mid, and root) to determine the hardness profile and the hardness variation along the weld depth, Fig. 1a. The conventional flat transverse tensile specimens extracted from the joints

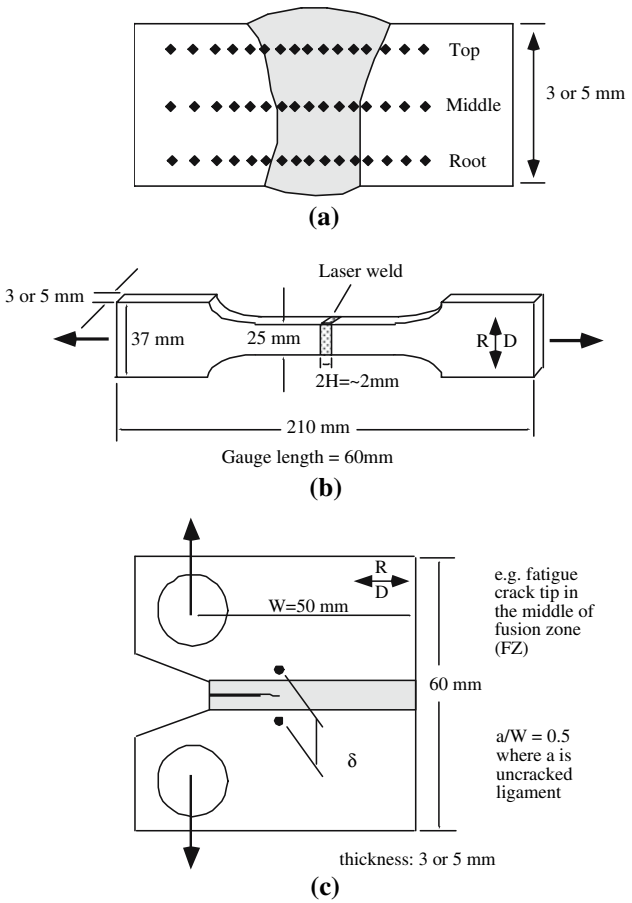

Fig. 1 Schematic showing: (**a**) hardness measurements, (**b**) tensile test specimens, and (**c**) compact tension (CT) specimen with local crack tip opening displacement (CTOD) measurement technique of δ_5. (Note: CTOD fracture toughness is directly measured by δ_5 clip-on-gauge as shown)

without machining the weld profile were tested at room temperature with a loading rate of 0.5 mm/min, Fig. 1b, to determine the mechanical properties of the joint. Standard compact tension (CT) specimens were also extracted from the joint, Fig. 1c, and cracked in the FZ and HAZ to determine the local fracture toughness properties. The crack tip opening displacement (CTOD) tests were performed on these specimens as well as on the base metal specimens at room temperature to determine the fracture toughness values (R-curves) of the base plate and the EB joint. Fracture toughness test specimens were investigated after testing by scanning electron microscopy to understand fracture behaviour of the joint and to determine the effect of microstructure and strength mismatch on the fracture behaviour.

Results and discussion

Microstructural and hardness aspects

A macrograph showing the cross-section of the EB joint is given in Fig. 2, which exhibits a very narrow fusion zone. A significant undercutting in the top region of the joint was observed in some plates.

Figure 3 shows scanning electron micrographs of the base material and the weld region. The base material has a microstructure consisting of elongated grains in the rolling direction containing some Fe-rich particles, possibly $Al_{15}Fe_3Si$ according to EDX results, white phases in Fig. 3a. A very narrow HAZ (overaged region) containing coarsened Mg_2Zn particles and some grain boundary liquation was also observed, Fig. 3b. The fusion zone exhibited distinct grain boundary formation decorated with Mg- and Zn-rich particles. Mg- and Zn-rich particles were observed along the grain boundaries as well as within the grains, white phases in Fig. 3c. The SEM/EDX study indicated that this phase has a 13.5% higher Zn concentration than the matrix phase and also 4.5% higher Mg concentration than the matrix, and assumed to be non-stoichiometric Mg_2Zn. The grain boundary regions contain α-Al and intermetallic Mg_2Zn. This intermetallic phase has a hexagonal structure [8]. No porosity was detected in the fusion zone by scanning electron microscopy which is inherent to electron

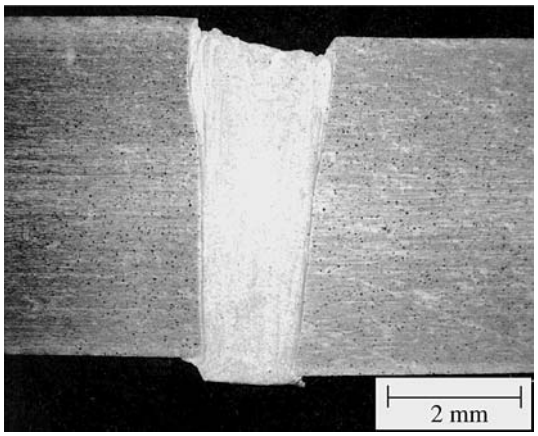

Fig. 2 Macrograph of alloy 7020 EB joint. Note: undercutting and misalignment

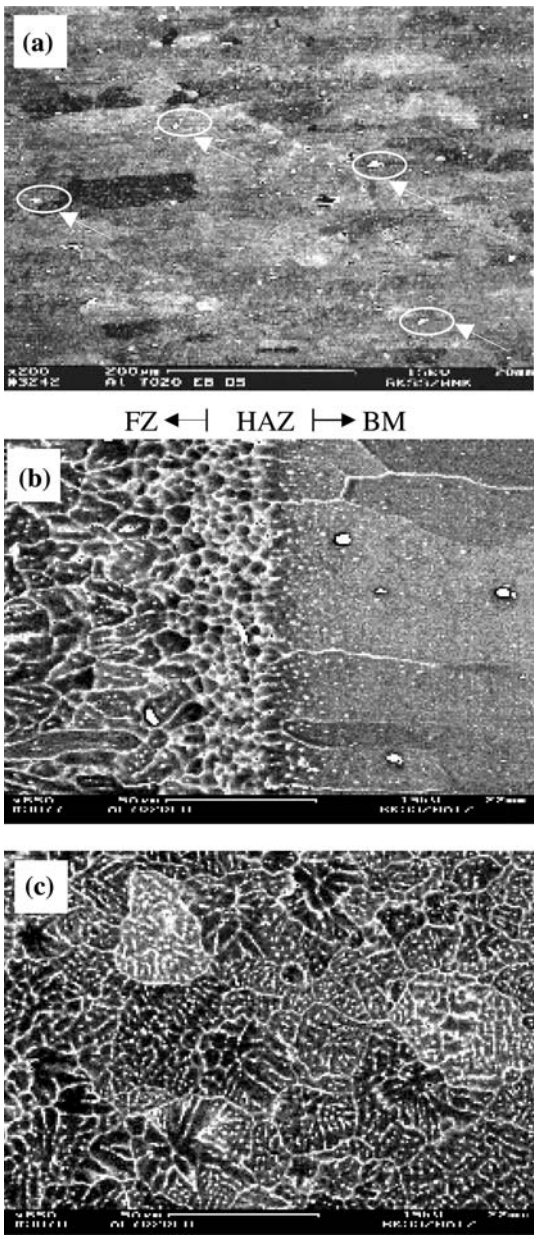

Fig. 3 SEM micrographs showing: (**a**) BM microstructure with some precipitates, possibly $Al_{15}Fe_3Si$ (white phases indicated by white circles and arrows), (**b**) the transition region between BM and FZ (note particle coarsening on the BM side), and (**c**) FZ microstructure containing Mg- and Zn-rich precipitates (white phases) along the grain boundaries and within the grains

beam welding process [9]. Optical microscopy also did not reveal any indication of the presence of pores in the fusion zone, Fig. 4.

Figure 5 shows the hardness profile of the joint. A significant hardness decrease was observed in the fusion zone. No significant hardness reduction was observed in the very narrow HAZ region compared to the base material. The reason for this is the rapid cooling involved in the EB welding which leads to a less pronounced particle growth in the HAZ due to the shortened overaging, compared to the conventional arc welding of this alloy where the formation of a wider HAZ with coarser particles and consequently a significant hardness loss in the HAZ are expected due to prolonged overaging [3].

EDX point analyses indicated that the matrix phase in both FZ and HAZ contain less Zn than the base plate matrix as expected, Table 1. This is due to the formation of Mg and Zn-rich particles, i.e. Mg_2Zn, along the grain boundaries and within the grains in the FZ, Fig. 3c, and the coarsening of Mg_2Zn particles in the narrow HAZ region (see the extent of the large particles in the narrow HAZ, Fig. 3b).

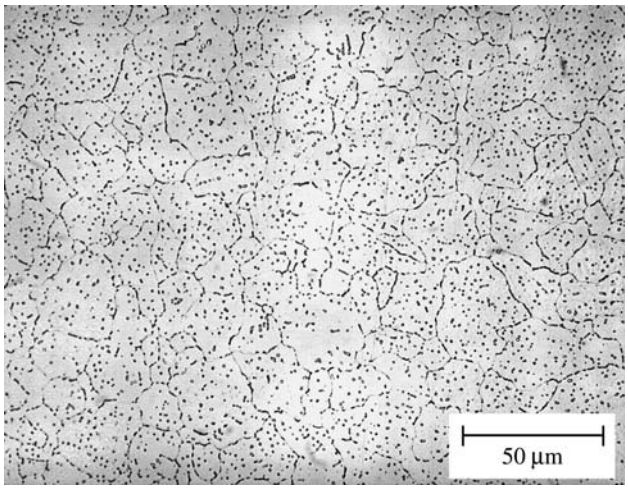

Fig. 4 Optical micrograph of the FZ exhibiting no porosity

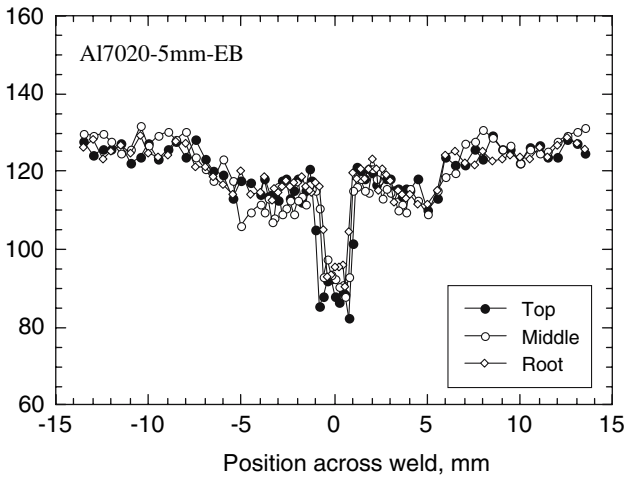

Fig. 5 Hardness profile of alloy 7020 EB joint

EDX analyses also showed that the Si contents of BM and FZ are similar indicating no loss of this element during welding. EDX area analyses (sampling large enough area which accounts for Mg and Zn distributions) were also conducted in the FZ and BM to determine any loss of these elements. In these area analyses, the Mg and Zn contents of the FZ were detected to be similar to those of the BM, suggesting no appreciable loss of these elements from the weld pool during welding. Cieslak and Fuerschbach [7] reported Mg evaporation during laser beam welding of alloy 6061 and proposed that it may lead to loss of strength in the fusion zone. However, they only measured the Mg loss in the short transverse direction (i.e. where the laser beam impinged), thus not representing the bulk composition of the base plate. Therefore, it is believed that the microstructural change (formation of large non-strengthening Mg_2Zn particles along the liquated grain boundaries) taking place in FZ and the resulting loss of solid solution strengthening due to Mg depletion in the FZ matrix phase can be the reason for the hardness loss in the fusion zone. Similar observations were also made in other EB welded Al-alloys, such as alloys 2024 and 6061 [10, 11].

Tensile properties

Standard flat transverse tensile specimens were tested to determine the mechanical properties and joint efficiency of the joint. The welded plates were tested with their original weld profiles. The reason for this is to determine the properties of as-welded plate although this will introduce stress concentration. The results are summarized in Table 2, which also includes the base metal properties determined by testing transverse tensile specimens (perpendicular to the rolling direction). All the joints failed in the weld region due to the lower strength in this region compared to the base material (see the hardness profile, Fig. 5). The strength of this alloy is derived from solid solution strengthening and/or precipitation hardening and the dissolution of alloying elements and/or the formation of large non-strengthening particles lead to a decrease in strength of the FZ since the barriers to the flow of dislocations become less.

Transverse tensile test results showed a significant loss of ductility in the joint, Fig. 6, which is very usual in power beam welded precipitation strengthened Al-alloys [2, 3, 10, 11]. This is due to strain concentration (confined plasticity) in the lower strength fusion zone resulting from the loss of strength as expected from the hardness profile of the joint,

Table 1 EDX point analyses results

Specimen	Elements	Al	Cu	Mg	Si	Fe	Cr	Zn	Mn
Matrix									
BM	wt%	93	–	2	1	–	–	**4**	–
	at%	95	–	2	1	–	–	2	–
HAZ	wt%	95	–	2	1	–	–	**2**	–
	at%	96	–	2	1	–	–	1	–
FZ	wt%	95	–	2	1	–	–	**2**	–
	at%	96	–	2	1	–	–	1	–
Precipitates									
BM	wt%	62	8	1	6	18	2	2	1
	at%	75	4	1	6	11	1	1	1
HAZ	wt%	83	1	2	3	6	–	5	–
	at%	89	1	3	3	2	–	2	–
FZ	wt%	73	2	6	3	–	–	16	–
	at%	81	1	8	3	–	–	7	–

BM contains more Zn than the FZ and HAZ in the matrix phase, but the Mg and Zn content of the precipitates in the FZ and HAZ are greater than those of the BM but the Cu-content is lower

Table 2 Results of tensile tests (values are average of 3 specimens)

Material	$R_{p0.2}$ Yield strength (MPa)	R_m Tensile strength (MPa)	A elongation (%)	Joint efficiency in terms of R_m (%)	Joint efficiency in terms of A (%)
Al7020 (BM)	326	385	13.6	–	–
Al7020 (EBW)	262	343	3.7	89.1	27.2

Fig. 5, in addition to the geometrical effect (undercutting), Fig. 2. This is the reason for the very low joint efficiency in terms of elongation, i.e. about 26%. However, the joint efficiency in terms of tensile strength was found to be reasonably high, i.e. about 89%, although there is a significant undercutting which reduces the strength of the welds.

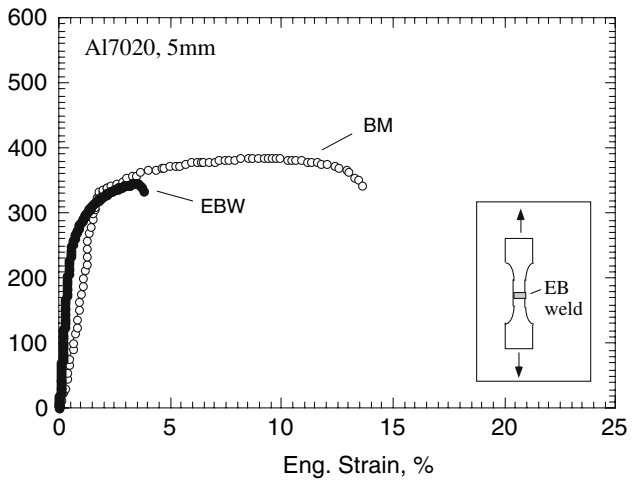

Fig. 6 Stress–strain curves of the base plate alloy 7020 and the EB joint

Fracture toughness

The results of fracture toughness tests conducted on base material and specimens extracted from the joints with different crack positions, i.e. FZ- and HAZ-cracked, are summarized in Table 3. The base material specimens exhibited the lowest fracture toughness value, i.e. CTOD (δ_5) = 0.38 mm. The FZ-cracked specimens displayed fracture toughness values, i.e. 0.44 mm, higher than that of the base material, but slightly lower than HAZ-cracked specimens, 0.49 mm (see Fig. 7 for specimen types). The R-curves of the BM, FZ, and HAZ are shown in Fig. 8. These results indicate that FZ and HAZ have significantly higher fracture toughness than the base material and thus displayed higher resistance to stable crack growth, Table 3.

Table 3 CTOD fracture toughness values

CTOD$(\delta_5)_m$ [mm]			
Material	Base material (BM)	Fusion zone (FZ)	Heat affected zone (HAZ)
Al 7020 T6	0.412	0.549	0.506
	0.389	**0.439**	0.547
	0.394	0.502	**0.485**

Bold values represent the minimum of three specimens tested

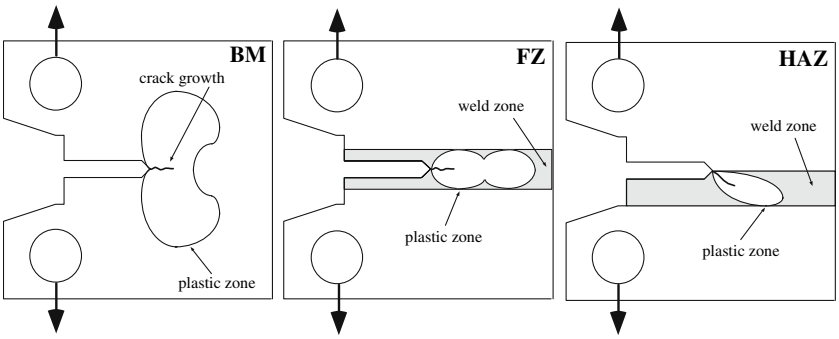

Fig. 7 Schematic illustration of the plasticity development in BM, FZ, and HAZ specimens. Note confined plasticity development within the lower strength FZ which increases the constraint at the crack tip region. Also note crack path deviation into FZ in HAZ-notched specimen

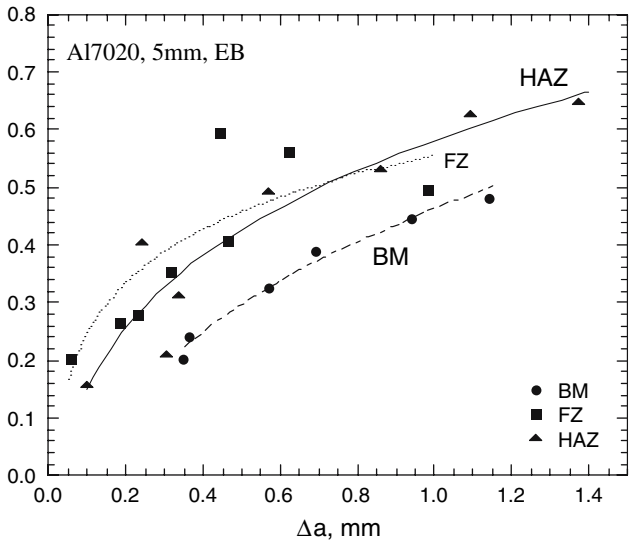

Fig. 8 CTOD R-curves of the base plate, FZ and HAZ-notched specimens. Higher toughness values of FZ and HAZ are due to strength undermatching

This is not surprising due to the fact that the loss of strength in the fusion zone naturally leads to an increase in the fracture toughness value, which is a well-known phenomenon in Al-alloys joints [10, 11].

Figure 9 shows the crack deviation into lower strength FZ during fracture toughness testing of a HAZ-cracked specimen, which is the reason for the similar R-curve behaviour exhibited by FZ- and HAZ-cracked specimens. The asymmetric and confined plasticity developments in FZ and HAZ fracture toughness specimens, respectively, compared to the BM specimen are shown schematically in Fig. 7. Fig. 10 shows the stable (ductile) crack growth process in the FZ zone involving the coalescence of developed pores with the growing crack during fracture toughness testing. Fig. 11 also shows the fracture surface of a transverse tensile specimen where the crack coalescence is visible.

The SEM study demonstrated that the crack growth within the FZ takes place along the grain boundaries, which contain brittle intermetallic particles presenting a

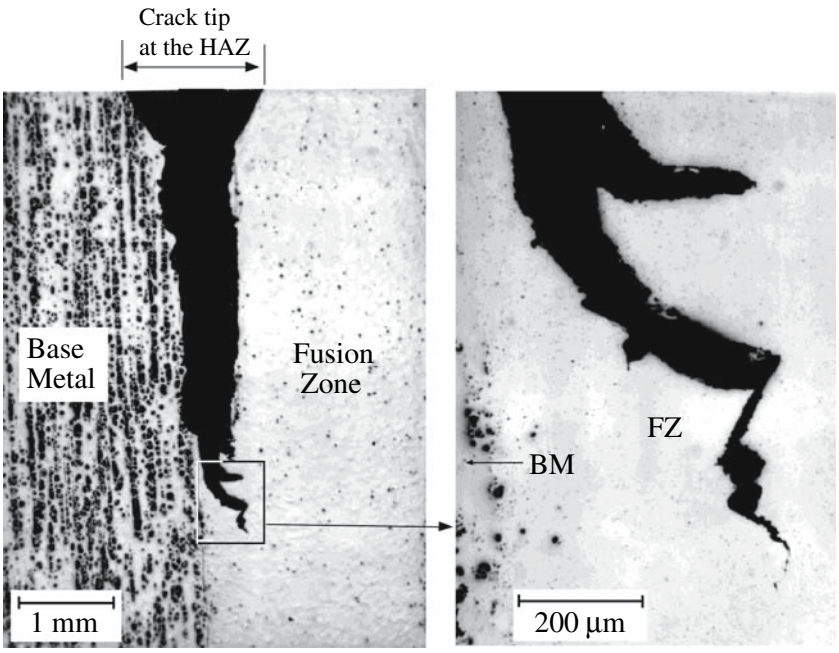

Fig. 9 Optical micrographs showing the crack (HAZ-crack) path deviation into lower strength fusion zone in a compact tension (CT) specimen

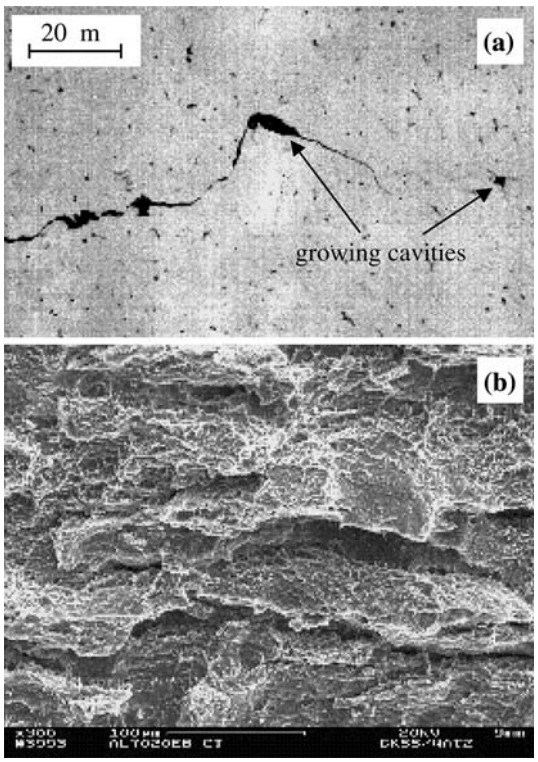

Fig. 10 Micrographs of the crack growth in FZ: (**a**) optical micrograph showing the crack growth by coalescence of cavities in a CT specimen and (**b**) SEM micrograph of the corresponding fracture surface (intergranular fracture)

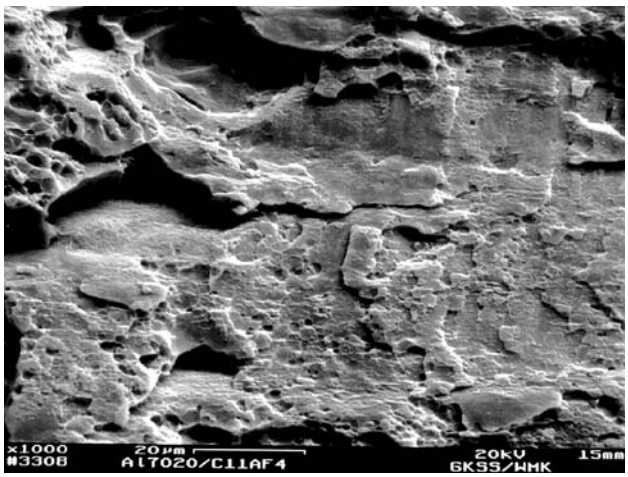

Fig. 11 SEM micrograph showing fracture surface of transverse tensile specimen failed in the fusion zone (intergranular fracture)

favourable crack path, Fig. 12. At the ahead of the crack, voids form along these boundaries containing brittle particles under the external load. These newly formed voids grow and coalesce with the main crack with increasing external load, Fig. 10. The nucleation of a crack within the grain is usually hindered by the presence of brittle grain boundaries contributing to the crack growth along the

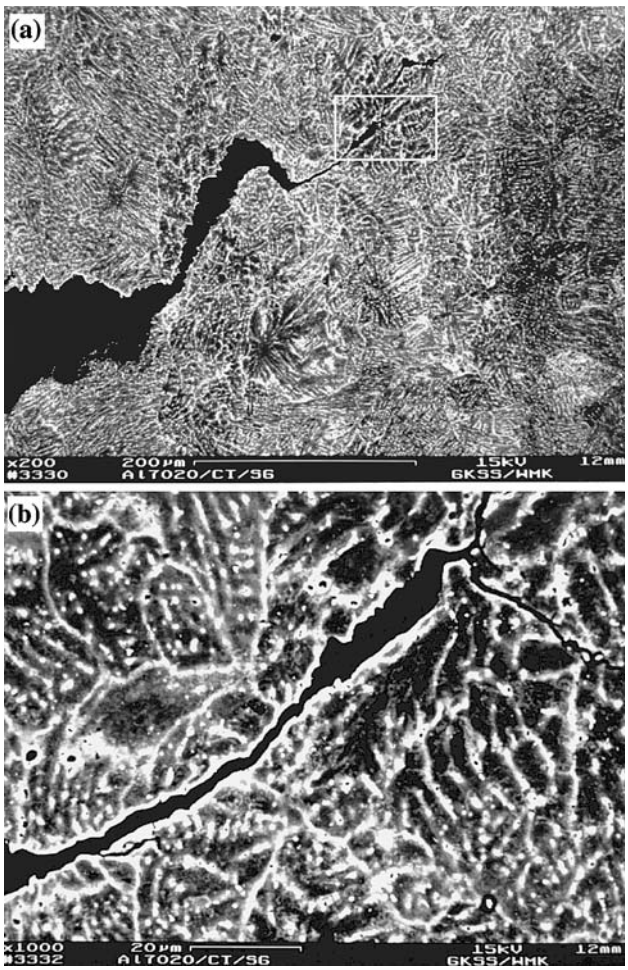

Fig. 12 SEM micrographs showing: (**a**) crack growth in the FZ and (**b**) high magnification of the region marked by white rectangular in (**a**) illustrating the crack growth along the grain boundary

brittle grain boundaries as observed in the FZ of this weldment leading to intergranular fracture occurring along liquated grain boundaries, Fig. 12. Although the crack growth along the brittle grain boundaries may seem to decrease fracture toughness of the FZ, this process as well as the crack blunting due to the nucleation of slip lines within the soft grains at the vicinity of the crack tip are both energy dissipating processes and increase the fracture toughness of the FZ, Table 3.

Conclusions

The following conclusion have been drawn from the present work:

- Crack-free welds in alloy 7020 was produced by EB welding. However, undercutting and joint mismatch were observed in some of the welded plates.

- The fusion zone exhibited the minimum hardness. This is believed to be due to the microstructural changes (i.e. the redistribution of Mg and Zn and consequently the formation of large intermetallic Mg_2Zn particles along the grain boundaries leading to Mg dilution in the matrix), rather than due to the loss of alloying elements.
- Transverse tensile test results showed a slight decrease in strength and a significant loss of ductility in the joint. The joint efficiency in terms of tensile strength was found to be about 89% whereas the joint efficiency in terms of elongation was very low, i.e. about 26%, due to strain concentration (confined plasticity) in the narrow lower strength fusion zone (about 1.5 mm width).
- The FZ and HAZ exhibited higher fracture toughness than the base material and thus displayed higher resistance to stable crack growth due to strength undermatching. Intergranular fracture occurring along the liquated grain boundaries was observed in the FZ.

Acknowledgements This work is a part of the Brite Euram AS-POW project (BRPR95-0021). Authors wish to thank the European Commission for the financial support. Thanks are also due to Mr. S. Riekehr, Mr. H. Mackel, and Mr. V. Ventzke for their assistance in conducting the experimental work. They would also like to thank Mr. G. Jennequin and Mr. P. Gonthier-Maurin of CNIM, La Seyne-Sur-Mer Cedex, France, where electron beam welding was performed.

References

1. Kuo S (1986) Welding research council bulletin, no. 320, WRC, New York
2. Çam G, Koçak M (1998) Sci Technol Welding Joining 3(4):159
3. Çam G, dos Santos JF, Koçak M (1997) Laser and electron beam weldability of Al-alloys: literature review. GKSS 97/E/25, GKSS Research Center, Geesthacht, Germany, IIW Doc. IX-1896-98
4. Çam G, Koçak M (1998) Int Mater Rev 43(1):1
5. Olson DL et al (eds) (1993) ASM handbook: welding, brazing, and soldering, vol 6. ASM International, Materials Park, Ohio
6. Murphy JL, Huber RA, Lever WE (1990) Weld J Res Suppl 69(4):125s
7. Cieslak MJ, Fuerschbach PW (1988) Metall Trans B 19B:319
8. Petrov DA (1993) In: Petzow G, Effenberg G (eds) Ternary alloys, vol. 7. VHC Publishers, New York, p 57
9. Rao SRK et al (2005) Mater Charact 55:345
10. Çam G et al (1999) J Sci Technol Welding Joining 4(5):317
11. Çam G et al (2000) Practical Metallography 37(2):59, also available as GKSS Report, GKSS 2000/9, GKSS Research Center, Geesthacht, Germany, 2000